Preprints, *25th Intern. Conf. on Interactive Information and Processing Systems*, Phoenix, AZ, Amer. Meteor. Soc., January 2009

# 9B.3 Progress Report on the Evolutionary Characteristics of a Tornadic Supercell Thunderstorm: Comparisons of 1.0–Min Phased Array Radar and 4.2–Min WSR–88D Measurements

RODGER A. BROWN
NOAA/National Severe Storms Laboratory, Norman, OK

JAMES M. KURDZO
Department of Earth Sciences, Millersville University, Millersville, PA

PAMELA L. HEINSELMAN
Cooperative Institute for Mesoscale Meteorological Studies
University of Oklahoma, Norman, OK

## 1. INTRODUCTION

Although a supercell thunderstorm may last for several hours, evolutionary processes within the storm—especially those related to the formation of microbursts and tornadoes—can occur on the scale of a few minutes. With the operational WSR-88D Doppler radar collecting volume scans at 4– to 6–min intervals, the initiation and descent of hazardous conditions is difficult to monitor. Unlike the WSR–88D, which uses a mechanically scanned beam, the electronically scanned beam of a phased array radar (PAR) permits greater scanning versatility and can collect 1–min volume scans in 90° sectors (e.g., Heinselman et al. 2008).

In late 2003, a 9.4–cm–wavelength (S–band) phased array Doppler radar became operational at the National Weather Radar Testbed in Norman, Oklahoma (e.g., Zrnić et al. 2007). The radar's 3.66–m–wide flat–plate antenna consists of 4352 transmit–receive elements. When the beam is perpendicular to the plate, the half–power beamwidth is 1.5°. When the beam is ±45° from the perpendicular, the beamwidth is 2.1°. Since the beamwidth varies as the inverse cosine of the angle from the perpendicular, the beamwidth is essentially uniform (1.5–1.7°) within ±30° of the perpendicular. In comparison, the *effective* horizontal beamwidth of a WSR–88D is approximately 1.4° for 1.0° azimuthal sampling (e.g., Brown et al. 2002).

During the early afternoon of 24 May 2008, a tornadic supercell thunderstorm entered southern Garfield County in north-central Oklahoma and moved slowly eastward along the county's southern border. Between approximately 1930 and 2230 UTC, a series of about 8 tornadoes were associated with the storm. Damage surveys indicated tracks ranging from 0.1 km to 16 km in length.

During the period that tornadoes were being produced, the storm was scanned by the PAR and the WSR–88D KTLX radar that is located about 20 km to the northeast of the PAR (Fig. 1). The PAR initially collected 45°–wide volume scans, centered on the storm, every 0.5 min. Collection had been changed to 90°–wide volume scans every 1.0 min prior to the time period discussed in this paper. KTLX completed full 360° volume scans in 4.2 min.

In this paper, we present some preliminary comparisons of the 1.0–min PAR and 4.2–min KTLX measurements during the time period that the longest-lasting tornado was occurring. At the time that this paper was written, not all of the radar characteristics of the storm had been analyzed. The results of more thorough analyses will be presented at a later date.

## 2. METHOD

During the time period that KTLX scanned the supercell storm, data were collected using Volume Coverage Pattern 12 (e.g., Brown et al. 2005). Each 360° volume scan consisted of 14 elevation angles (0.5, 0.9, 1.3, 1.8, 2.4, 3.1, 4.0, 5.1, 6.4, 8.0, 10.0, 12.5, 15.6, and 19.5°) that were collected at 4.2–min intervals. Data were collected at 1.0° azimuthal intervals. Doppler velocity data were collected and displayed at range intervals of 0.25 km, while the reflectivity data were averaged over four 0.25–km–range intervals and displayed at 1.0–km intervals.

For its 45°– and 90°–wide (0.5 min and 1.0 min) volume scans, the PAR collected data at the following 14 elevation angles: 0.5, 1.1, 1.7, 2.4, 3.2, 4.1, 5.1, 6.2, 7.4, 8.7, 10.1, 11.7, 13.5, and 15.5°. Between the 5.1 and 6.2° elevation angles, the radar made a second 0.5° elevation scan. Reflectivity and Doppler velocity data were collected at 1.0° azimuthal intervals and 0.235 km range intervals. With electronic scanning, the PAR is not subject to the azimuthal smearing of data that is a characteristic of mechanically scanned radars like the WSR–88D.

Though a single Doppler radar does not measure the three–dimensional flow field within a severe thunderstorm, Doppler velocity and reflectivity signatures help to deduce important supercell thunderstorm dynamics. The presence of rotation in a storm produces a unique single Doppler velocity signature. The mesocyclone, which provides the

*Corresponding author address*: Dr. Rodger A. Brown, National Severe Storms Laboratory, 120 David L. Boren Blvd., Norman, OK 73072. E-mail: Rodger.Brown @noaa.gov.

necessary background cyclonic vorticity for tornado formation in a supercell storm, is revealed in single Doppler velocity data by a region of pronounced flow away from the radar located in a clockwise azimuthal direction from a region of pronounced flow toward the radar. The mean rotational velocity was computed by taking one–half of the difference between maximum flow away from the radar (typically positive) and maximum flow toward the radar (typically negative). Though there is considerable variability from mesocyclone to mesocyclone, mean rotational velocities characteristically are of the order of 25 m $s^{-1}$ and core diameters (distance between maximum flow toward and away from the radar) characteristically are of the order of 5 km (e.g., Burgess et al. 1982).

The tornado is such a small rotating phenomenon that—when the radar beam is wider than the tornado—the peak values of the resulting tornadic vortex signature (TVS) are approximately one beamwidth apart regardless of tornado size (e.g., Brown et al. 1978). This means that, for a radar that has a beamwidth of 1.0–1.5$^{o}$ and that collects velocity data at azimuthal intervals of 1.0$^{o}$, the peak Doppler velocity values representing flow toward and away from the radar typically are found at adjacent azimuths. In those less common situations when the radar beam is centered on the tornado, the extreme Doppler velocity values are two azimuthal intervals apart. For the preliminary TVS data presented in this paper, the Doppler velocity difference across the TVS was taken as the difference between two adjacent azimuths (sometimes called gate–to–gate differences). Later, the Doppler velocity differences will be reevaluated by manually fitting the Doppler velocity measurements to theoretical TVS curves in order to estimate the difference between the *peak* Doppler velocity values derived from the curves, rather than using the simpler gate–to–gate values (Brown 1998).

Doppler radar measurements contain several reflectivity signatures that are useful in deducing relative updraft strengths. These signatures include the bounded weak echo region (BWER), evolution of maximum reflectivity at midaltitudes, and the vertical extent of individual updraft/downdraft cells. The BWER is present when an updraft is so strong that hydrometeors do not have time to grow to radar–detectable sizes until they are well up into the storm. Reflectivity values greater than 55–60 dBZ at midaltitudes indicates the likely presence of hail and therefore the presence of strong vertical velocities that are needed to suspend the growing hailstones. Analyses of these two signatures have not yet been completed and therefore are not presented here.

The vertical extent of individual updraft/downdraft cells provides an indication of relative strength of sequential updrafts within a storm (e.g., Brown and Meitín 1994; Brown and Torgerson 2003). We found that the evolution of an individual cell top could best be depicted by following its 30–dBZ surface. Two different situations had to be considered: (a) when reflectivity was less than 30 dBZ at the highest elevation angle with data and (b) when reflectivity was greater than 30 dBZ at the highest data level. We noted that, in the upper part of the Garfield County storm, reflectivity decreased linearly at an average rate of about 8.5 dBZ $km^{-1}$ (typical range of 7.5–9.5 dBZ $km^{-1}$) with increasing height. This fact made it possible to determine the height of the 30–dBZ surface (a) by linearly interpolating the height using reflectivity values at the two top elevation angles with data or (b) by linearly extrapolating the reflectivity from the top data level up to the 30–dBZ height.

## 3. PRELIMINARY RESULTS

The times of tornado occurrence associated with the 16–km–long damage track were not available from the damage survey. Consequently, times were estimated by comparing Doppler velocity and reflectivity signatures with the geographical locations of the beginning and ending of the damage track. It appears that the tornado touched down at approximately 2130–2135 UTC and lifted at approximately 2215–2220 UTC.

Variations in the heights of the 30–dBZ tops of updraft/downdraft cells in the Garfield County supercell storm in Fig. 2 reveal the waxing and waning nature of the storm during the time of the 16–km–long tornado track. One gets the impression that the 1.0–min PAR data reveal the existence of individual turrets at storm top, while the less–detailed resolution of the 4.2–min KTLX data presents a smoothed overview. The KTLX cell tops are lower than the PAR tops for several reasons. The most likely reason is that KTLX reflectivity values are displayed as the 1.0–km average of four consecutive 0.25 km range gates, whereas the PAR values are those measured at individual 0.235 km gates. With the coarser temporal sampling of KTLX, it is probable that some of the true peak values were missed. There also is the possibility that there were calibration differences between the two radars.

The KTLX and PAR data in Fig. 2 show updrafts (cells) reaching lesser heights (suggesting slightly weaker updrafts) and a decrease in updraft activity around 2135 UTC. After recovering, there was a briefer decrease in heights of the PAR–detected cells around 2148 UTC. After about 2205 UTC, PAR data indicate that there was a gradual decline in the strength of successive updrafts until about 2228 UTC, after which the PAR measurements indicate an increase in heights.

The mesocyclone data in Fig. 3 indicate that there were two time periods with stronger rotational velocities. The first period, up through about 2135 UTC, was quite variable. Following a period of weaker rotational velocities through about 2142 UTC, more consistent rotational velocities were present through about 2207 UTC. It is interesting that the intermediate period with weaker rotational velocities around 2135 UTC coincides with the weaker updrafts (shorter 30–dBZ cell tops). It may be noted that the PAR data provide much more detail about mesocyclone evolution than do the KTLX data.

Likewise, the PAR data in Fig. 4 provide more details about TVS evolution. For example, between 2130 and 2135 UTC a strong TVS was detected aloft

and it increased in vertical extent as it approached the ground. This likely marked the beginning of the tornado that produced the 16–km–long damage track. However, for some reason, as indicated by the gray region, it was not possible to detect evidence of the tornado for the next 3–4 min even though a region of marked cyclonic shear remained. The gray region corresponds to the same time period when the mesocyclone signature was weak and when the updrafts appeared to be weaker. Both the PAR and KTLX TVS values also were noticeably weaker from about 2151 to 2159 UTC.

There are suggestions in the TVS time–height plots and in the apparent evolution of the low–altitude reflectivity hook echo (not shown) that the 16–km–long damage track may have been produced by more than one tornado. With a slowly moving storm passing over rural areas, it would be difficult to know whether sparse damage along a given damage track was produced by one or by more than one tornado. As mentioned earlier, we will be re-evaluating the PAR TVS data by fitting the data to theoretical TVS Doppler velocity curves (Brown 1998). In this way, we expect the more consistent TVS differences to reveal whether the 16–km–long damage track was produced by one or more than one tornado.

## 4. DISCUSSION

It is clear from the data presented in Figs. 2–4 that the 1.0–min PAR data provide a much more detailed picture of the processes taking place within a tornadic storm than do the 4.2–min KTLX data. Consequently, one can identify and interpret storm features with greater confidence.

VCP 12 used by KTLX for this study is the fastest of the scanning strategies available to WSR–88D radars. The other precipitation scanning strategies take 5–6 min to complete a volume scan. Therefore, this study provides the most favorable comparison of a WSR–88D radar with the PAR.

There was a relatively narrow Nyquist co–interval of ±23.8 m $s^{-1}$ used to collect PAR Doppler velocity data for this particular study, meaning that velocity values that exceeded ±23.8 m $s^{-1}$ were aliased back into the ±23.8 m $s^{-1}$ velocity interval. With such a narrow Nyquist co–interval, the automated dealiasing algorithm had problems properly dealiasing all of the data. Consequently, all of the Doppler velocity data had to be examined and dealiased manually wherever aliasing problems occurred. The gray regions in Fig. 4 contained aliased data that were impossible to properly interpret. During the Spring 2009 data collection period, a staggered pulse repetition time (PRT) technique will be implemented on the PAR (e.g., Torres et al. 2004). This technique will mitigate most Doppler velocity aliasing as well as range folding ambiguities in the data.

## 5. ACKNOWLEDGMENTS

The second author was supported by an appointment to the National Oceanic and Atmospheric Administration (NOAA) Research Participation/Hollings Scholarship Program through a grant awarded to Oak Ridge Institute for Science and Education. Funding for the third author was provided by NOAA/Office of Oceanic and Atmospheric Research under NOAA–University of Oklahoma Cooperative Agreement NA17RJ1227. We thank Joan O'Bannon for skillfully drafting Fig. 2.

## 6. REFERENCES

Brown, R. A., 1998: Nomogram for aiding the interpretation of tornadic vortex signatures measured by Doppler radar. *Wea. Forecasting*, **13**, 505–512.

_____, and R. J. Meitín, 1994: Evolution and morphology of two splitting thunderstorms with dominant left–moving members. *Mon. Wea. Rev*., **122**, 2052–2067.

_____, and K. L. Torgerson, 2003: Interpretation of single–Doppler radar signatures in a V–shaped hailstorm: Part I—Evolution of reflectivity–based features. *Natl. Wea. Digest*, **27**, 3–14.

_____, L. R. Lemon, and D. W. Burgess, 1978: Tornado detection by pulsed Doppler radar. *Mon. Wea. Rev*, **106**, 29–38.

_____, V. T. Wood, and D. Sirmans, 2002: Improved tornado detection using simulated and actual WSR–88D data with enhanced resolution. *J. Atmos. Oceanic Technol*., **19**, 1759–1771.

_____, R. M. Steadham, B. A. Flickinger, R. R. Lee, D. Sirmans, and V. T. Wood, 2005: New WSR–88D volume coverage pattern 12: Results of field tests. *Wea. Forecasting*, **20**, 385–393.

Burgess, D. W., V. T. Wood, and R. A. Brown, 1982: Mesocyclone evolution statistics. Preprints, *12th Conf. on Severe Local Storms*, San Antonio, TX, Amer. Meteor. Soc., 422–424.

Heinselman, P. L., D. L. Priegnitz, K. L. Manross, T. M. Smith, and R. W. Adams, 2008: Rapid sampling of severe storms by the National Weather Radar Testbed phased array radar. *Wea. Forecasting*, **23**, 808–824.

Torres, S. M., Y. F. Dubel, and D. S. Zrnić, 2004: Design, implementation, and demonstration of a staggered PRT algorithm for the WSR–88D. *J. Atmos. Oceanic Technol*., **21**, 1389–1399.

Zrnić, D. S., J. F. Kimpel, D. E. Forsyth, A. Shapiro, G. Crain, R. Ferek, J. Heimmer, W. Benner, T. J. McNellis, and R. J. Vogt, 2007: Agile–beam phased array radar for weather observations. *Bull. Amer. Meteor. Soc*., **88**, 1753–1766.

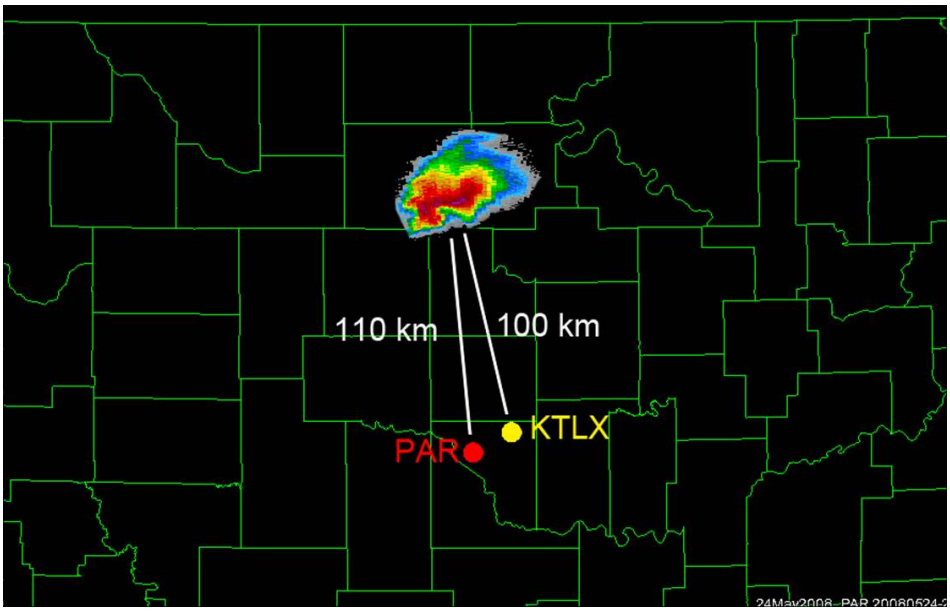


**Fig. 1**. Location of the Garfield County supercell thunderstorm relative to the phased array radar (PAR) and the KTLX WSR–88D radar at 2145 UTC.

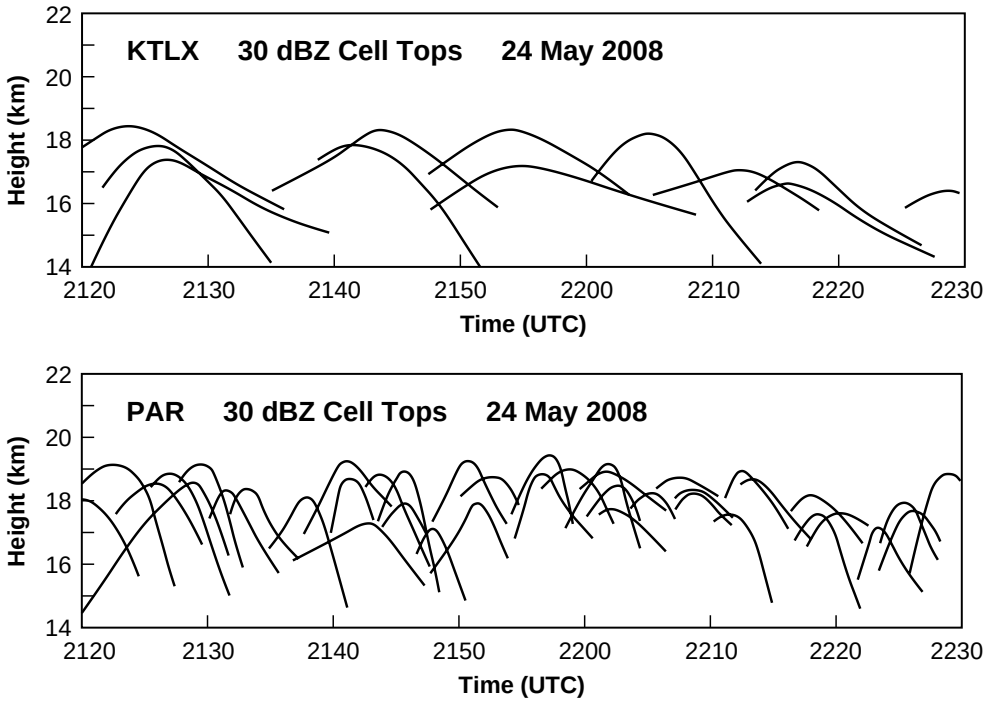


**Fig. 2**. Time–height plots of the 30 dBZ tops of individual updraft/downdraft cells as revealed by 4.2–min KTLX data (top) and 1.0–min PAR data (bottom).

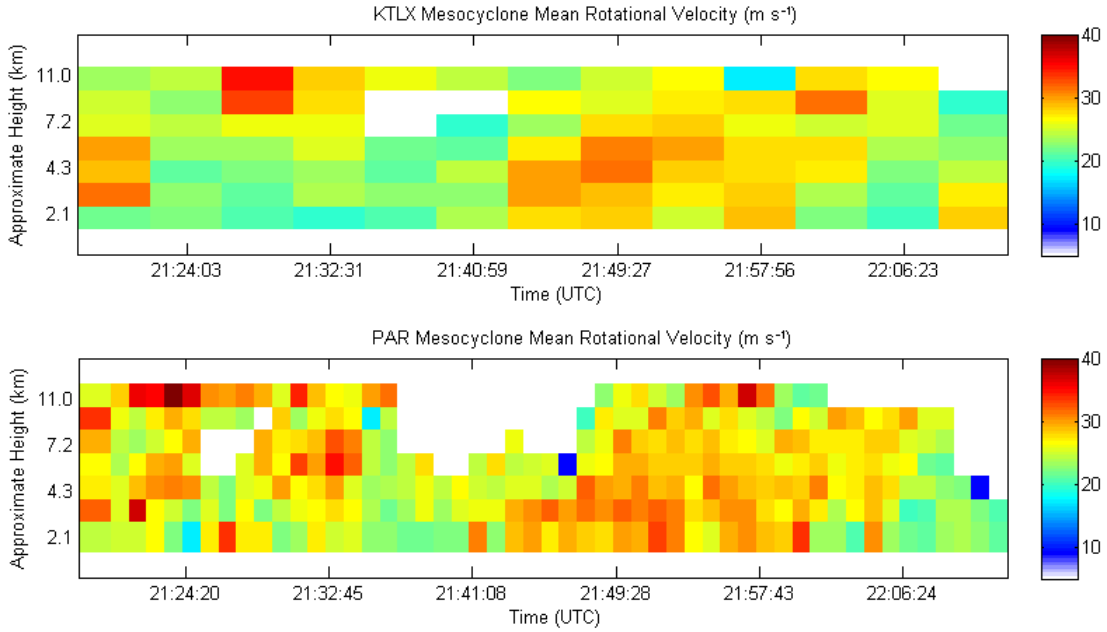


**Fig. 3**. Time–height plots of the mean mesocyclone rotational velocity (m $s^{-1}$) derived from the extreme Doppler velocity values toward and away from the radar associated with the single Doppler velocity mesocyclone signature. The color bar on the right indicates the strength of the mean rotational velocity based on 4.2–min KTLX (top) and 1.0–min PAR (bottom) measurements. White regions indicate that no mesocyclone signatures were present.

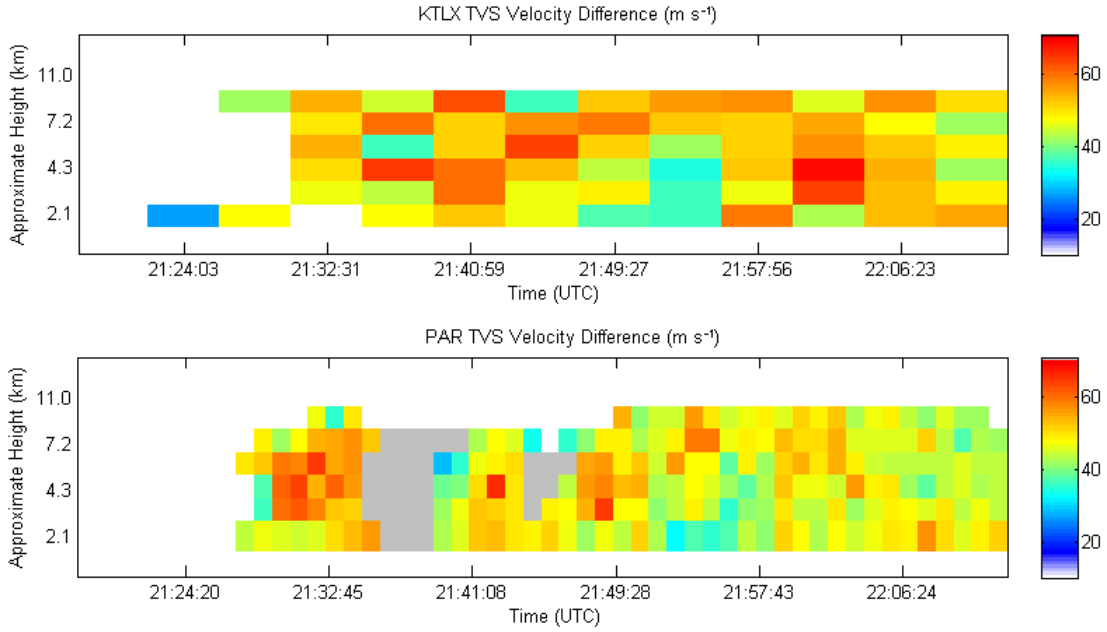


**Fig. 4**. Time–height plots of the gate–to–gate Doppler velocity difference (m $s^{-1}$) across the single Doppler velocity tornadic vortex signature (TVS). The color bar on the right indicates TVS strength based on 4.2–min KTLX (top) and 1.0–min PAR (bottom) measurements. Gray PAR regions indicate that TVS–scale cyclonic shear was present, but distinctive TVSs were not identifiable. White regions indicate that TVS–scale cyclonic shear was not present.